Loss of Hematopoietic Cell–Derived Oncostatin M Worsens Diet-Induced Dysmetabolism in Mice

Mattia Albiero,[1,2] Stefano Ciciliot,[2,3] Anna Rodella,[1,2] Ludovica Migliozzi,[1,2] Francesco Ivan Amendolagine,[1,2] Carlotta Boscaro,[1,2] Gaia Zuccolotto,[4] Antonio Rosato,[4,5] and Gian Paolo Fadini[1,2]

Diabetes 2023;72:483–495 | https://doi.org/10.2337/db22-0054

Innate immune cells infiltrate growing adipose tissue and propagate inflammatory clues to metabolically distant tissues, thereby promoting glucose intolerance and insulin resistance. Cytokines of the IL-6 family and gp130 ligands are among such signals. The role played by oncostatin M (OSM) in the metabolic consequences of overfeeding is debated, at least in part, because prior studies did not distinguish OSM sources and dynamics. Here, we explored the role of OSM in metabolic responses and used bone marrow transplantation to test the hypothesis that hematopoietic cells are major contributors to the metabolic effects of OSM. We show that OSM is required to adapt during the development of obesity because OSM concentrations are dynamically modulated during high-fat diet (HFD) and *Osm*$^{-/-}$ mice displayed early-onset glucose intolerance, impaired muscle glucose uptake, and worsened liver inflammation and damage. We found that OSM is mostly produced by blood cells and deletion of OSM in hematopoietic cells phenocopied glucose intolerance of whole-body *Osm*$^{-/-}$ mice fed a HFD and recapitulated liver damage with increased aminotransferase levels. We thus uncovered that modulation of OSM is involved in the metabolic response to overfeeding and that hematopoietic cell–derived OSM can regulate metabolism, likely via multiple effects in different tissues.

ARTICLE HIGHLIGHTS

- The role of oncostatin M (OSM) in the metabolic consequences of overfeeding is debated.
- We tested the hypothesis that hematopoietic cells are major contributors to the metabolic effects of OSM.
- Modulation of OSM is involved in the metabolic response to overfeeding, and hematopoietic cell–derived OSM can regulate metabolism.
- The coordinated release of OSM by blood cells is part of a physiological response to a high-fat diet, contributing to metabolic homeostasis.

Obesity is a major risk factor for insulin resistance and type 2 diabetes and represents a worldwide health burden (1). The expansion of adipose tissue (AT) during development of obesity elicits an acute sterile inflammatory response triggered by adipocyte death, local hypoxia, and mechanical stress (2) that stimulates recruitment of macrophages (3). This leads to a chronic low-grade inflammation that propagates to other metabolically relevant tissues, including liver (4).

Oncostatin M (OSM) belongs to the interleukin-6 (IL-6)/Gp130 family, which includes IL-6, IL-11, leukemia inhibitory factor (LIF), cardiotrophin-1, and ciliary neurotrophic factor. In humans, OSM binds the gp130/LIFRβ or the OSMRβ/gp130 complexes. In mice, OSM binds almost exclusively the OSMRβ/gp130 receptor (5). OSM intracellular signaling pathways include JAK2/STAT3, MAP kinases, and PI-3 kinase (6). OSM is produced by neutrophils, eosinophils,

[1]Department of Medicine, University of Padova, Padova, Italy
[2]Veneto Institute of Molecular Medicine, Padova, Italy
[3]Department of Molecular Medicine, University of Pavia, Pavia, Italy
[4]Veneto Institute of Oncology IOV - IRCCS, Padova, Italy
[5]Department of Surgery, Oncology and Gastroenterology, University of Padova, Padova, Italy

Corresponding author: Mattia Albiero, mattia.albiero@unipd.it; mattia.albiero@gmail.com

Received 17 January 2022 and accepted 2 January 2023

This article contains supplementary material online at https://doi.org/10.2337/figshare.21860142.

M.A. and S.C. contributed equally to this work.

and macrophages in mice and also by activated T cells in humans (6). It is associated with inflammatory diseases, such as lung inflammation, multiple sclerosis, and rheumatoid arthritis. In the bone marrow (BM), OSM regulates hematopoiesis, myelopoiesis, and hematopoietic stem cell (HSC) traffic (7,8) by instructing stromal cells of the hematopoietic niche to secrete Cxcl12 and retain HSCs within the BM (9,10).

OSM has been studied in the setting of obesity and type 2 diabetes for its role inhibiting adipogenesis (8,11) and for being associated with inflammation. Some reports show that *Osm* and *Osmrß* mRNA are upregulated in the AT of mice fed a high-fat diet (HFD) or $Lep^{Ob/Ob}$ mice (12). Yet, the causal meaning of such regulation is unclear because $Osmrß^{-/-}$ mice fed a HFD have a more severe metabolic phenotype than wild-type (Wt) controls (12,13). Macrophages accumulating within the stromal vascular fraction of AT during obesity have been described as the major source of OSM in humans and mice, whereas adipocytes were found to express and release little to no OSM (14). $Lep^{Ob/Ob}$ mice and HFD-fed mice treated with high-dose OSM displayed improved glucose tolerance, reduced hepatic steatosis, and attenuation of AT inflammation (12,15). In adipocyte-specific *Osmrß* knockout ($Osmr^{FKO}$) mice, HFD induced a mild phenotype characterized by increased AT inflammation (16,17). Conversely, inhibiting OSM with a polyclonal antibody reduced blood glucose in HFD-fed animals (18).

In the liver, OSM is mainly produced by Kuppfer cells (19), but its expression is not modified in $Lep^{Ob/Ob}$ or HFD mice (12). However, hepatic overexpression of OSMRβ or STAT3 blunted steatosis and insulin resistance in $Lep^{Ob/Ob}$ mice or after an HFD (20).

Reconciling these contrasting findings is challenging. Inconsistency of evidence is likely due to the diverse cellular sources of OSM, the broad expression of its receptors with different subunit combinations, and the resulting tissue-specific activities. In fact, insight gathered from studies on $Osmrß^{-/-}$ mice might be biased by OSM signaling through the LIF receptor at higher concentrations (21). Furthermore, mouse OSM requires LIFR? to modulate bone formation (22), which, in turn, can affect systemic glucose metabolism through the release of osteokines (23). Here, we tested the hypothesis that hematopoietic cells are a major source of circulating OSM that contributes to the regulation of systemic metabolism.

RESEARCH DESIGN AND METHODS

Animals

For all experiments we used male age-matched animals on a C57BL/6J background randomly assigned to the various experimental groups. For the HFD protocol, male mice at 8 weeks of age were randomly assigned to a standard diet (68% of calories from carbohydrates, 23.5% from proteins, 8.5% from fat) (4RF21; Mucedola, Milan, Italy) or an HFD (60% of calories from fat, 21% from carbohydrates, 19% from proteins) (EF acc. D12492 (I) mod.; Ssniff, Soest, Germany) for 12 weeks. Mice were housed with a maximum of 5 animals per cage with environmental enrichments at 23°C with a 12-h light/dark cycle. Additional details are provided in the Supplementary Materials. All studies were performed at the Veneto Institute of Molecular Medicine and were approved by the Veneto Institute of Molecular Medicine Animal Care and Use Committee (authorization no. 175/2002A), and by the Italian Health Ministry (authorization no. 310/2019-PR).

Metabolic Tests

Mice were fasted for 5 h before the tests. Basal glucose levels were measured and 1 g/kg D-glucose (for an intraperitoneal glucose tolerance test [ipGTT]) or 0.75 units/kg human recombinant insulin (for an intraperitoneal insulin tolerance test [ipITT]) was injected. Glycemia was measured at 30, 60, and 120 min after injection. HOMA of insulin resistance (HOMA-IR) was calculated as follows:

$$\text{HOMA-IR} = \frac{\left(\text{glucose}\left(\frac{\text{mmol}}{\text{L}}\right) \times \text{insulin}\left(\frac{\text{mU}}{\text{L}}\right)\right)}{22.5}.$$

For glucose uptake, mice were injected intraperitoneally with a 37:1 ratio of D-glucose (1 g/kg) to 2-deoxy-D-glucose (2DG; 0.027 g/kg) (Merck). After 1 h, mice were humanely sacrificed, and tissues were frozen in liquid nitrogen. Glucose uptake was measured using a 2DG Uptake Measurement Kit (Cosmo Bio Co., Ltd., Tokyo, Japan) as previously described (24).

Whole-Body Composition Analysis and Metabolic Cages

Whole-body lean mass and whole-body fat composition were determined with an EchoMRI 100 analyzer (EchoMRI, Houston, TX) in living and unrestrained animals. Animals were housed singly in TSE PhenoMaster cages (TSE Systems GmbH, Germany) at 23°C with a 12-h light/dark cycle for 24 h before measurement. VO_2, VCO_2, food intake, and water consumption were recorded for three consecutive days. The respiratory exchange ratio (RER) was calculated as VCO_2/VO_2 (25). Energy expenditure was calculated as follows:

$$\frac{3.941 \cdot VO_2 + 1.106 \cdot VCO_2}{1000}\left(\frac{\text{Kcal}}{\text{h} \cdot \text{Kg}}\right)$$

Flow Cytometry

BM cells were isolated by flushing femurs and tibias with ice-cold MACS Buffer (Miltenyi Biotec GmbH, Gladbach, Germany). AT and livers were processed as described (26). Cells were incubated with antibodies for 15 min at room temperature. Data were acquired with a FACSCanto (BD Biosciences) cytometer or sorted with a FACSCalibur cytometer followed by analysis using FlowJo software (BD Biosciences). The list of antibodies is provided in Supplementary Table 1.

Tissue and Peripheral Blood Analysis

Hematoxylin and eosin staining was performed on 4-μm-thick paraffin-embedded sections by standard methods.

Adipocytes count and area were determined using the SMASH plugin. Oil Red O (ORO) staining was performed as previously described (24). Masson's trichrome staining was performed using a commercially available kit (Bio-Optica, Italy). Peripheral blood triglyceride and cholesterol levels were measured using an Allegro analyzer (Nova Biomedical, Waltham, MA). Plasma free fatty acid levels were measured using a commercially available kit (ab65341; Abcam). AST was measured using the Adaltis Pchem2 Analyzer (Adaltis S.r.l., Italy). Liver lipids were extracted with a hexane-based method (ab211044; Abcam, Cambridge, UK) and quantified using enzymatic kits according to the manufacture's instruction (ab65336 and ab65359; Abcam). Plasma OSM was quantified with a commercial ELISA assay (R&D Systems, Inc.). Metabolic hormones and adipokines were quantified using a multiplex immunoassay (Mouse Diabetes 8-Plex; Bio-Rad Laboratories).

Macrophage Polarization

BM cells were obtained by flushing with sterile ice-cold PBS both femurs and tibia of 3-month-old mice. Macrophages were differentiated and polarized as previously described (10).

BM Transplantation

Mice received two 5-Gy doses 3 h apart, followed by an intravenous injection of BM cells (4×10^7/each). For BM reconstitution, animals were housed in sterile individually ventilated cages and provided sterile water and food. BM reconstitution was assessed 28 days after transplantation by performing flow cytometry and determining differential white blood cell and red blood cell counts, hemoglobin concentrations, and hematocrit on fresh EDTA-treated blood using the CELL-DYN Emerald analyzer (Abbott). No adverse events were recorded.

Molecular Biology

RNA was isolated using the Total RNA Purification Micro Kit (Norgen Biotek) and quantified with a NanoDrop 2000 Spectrophotometer (Thermo Fisher Scientific, MA). cDNA was synthesized using the SensiFAST cDNA Synthesis Kit (Bioline, London, UK). qPCR was performed using the SensiFAST SYBR Lo-ROX Kit (Bioline) via QuantStudio 5 Real-Time PCR System (Thermo Fisher Scientific).

Statistical Analysis

Data are reported as the mean ± SE for continuous variables. Normal distribution was checked using the Kolmogorov–Smirnov test. Non-normal continuous variables were log-transformed before analysis. Comparison of data between two or more groups was performed using a two-tailed unpaired Student *t* test or two-way ANOVA (with post hoc Bonferroni correction), respectively. Statistical significance was set at $P < 0.05$. GraphPad Prism 9.0 (GraphPad Software, La Jolla, CA) was used for data analysis. The number of biological replicates is reported in the figure legends or shown as individual data points in the figures. Outliers were determined using the robust regression and outlier removal (ROUT) method and removed if the false discovery rate was ≤ 0.01. Gene expression data were analyzed with gene set enrichment analysis (GSEA) software (Broad Institute).

Data and Resource Availability

All data generated or analyzed during this study are included in the published article and its online supplementary files.

RESULTS

OSM Source and Modulation During the Development of HFD-Induced Obesity

To identify the main sources of OSM within metabolically relevant tissues, we used FACS to isolate T lymphocytes ($CD45^+$ $CD3^+CD11b^-$ cells), neutrophils ($CD45^+CD3^-Ly6G/C^{bright}$ $CD11b^{bright}$ cells), and macrophages ($CD45^+CD3^-Ly6G/C^{mid}$ $CD11b^{bright}F4/80^+$ cells) from the AT and the liver (Fig. 1*A*). *Osm* expression was highest in neutrophils both in AT and liver. AT macrophages displayed greater *Osm* expression than did liver macrophages (Fig. 1*B*). By interrogating available single-cell RNA–sequencing data sets (27), we confirmed that neutrophils showed the highest *Osm* expression among mature leukocytes and their hematopoietic progenitors (Fig. 1*C*). *Osmr* was expressed at similar levels in the AT of Wt and $Osm^{-/-}$ mice, but its expression in the liver was lower than in AT, especially in $Osm^{-/-}$ mice (Fig. 1*D*). On the other hand, *Lifr* expression was significantly greater in liver than AT, irrespective of the genotype (Fig. 1*E*).

Next, we found that plasma OSM was markedly reduced after 12 weeks in Wt mice fed the HFD (Fig. 1*F*). Because this finding contrasts with some data from the literature (12), we assessed the dynamic changes of OSM concentrations during the development of obesity by a longitudinal analysis of glucose tolerance and plasma OSM in mice fed the HFD. Glucose tolerance rapidly deteriorated within 3–7 days after initiation of the HFD, then recovered partially before worsening again between 8 and 12 weeks (Fig. 1*G*). Plasma OSM peaked on day 14, when glucose tolerance started to improve, and then remained low during establishment of obesity and overt metabolic dysfunction.

Whole-Body *Osm* Deletion and Development of HFD-Induced Metabolic Perturbation

At 8 weeks of age, $Osm^{-/-}$ mice were 6.9% leaner than Wt mice (Fig. 2*A*) (body weight 24.33 ± 0.47 g vs. 22.63 ± 0.43 g; $P < 0.05$). Whole-body lean mass was slightly lower in $Osm^{-/-}$ than in Wt mice, without gross evidence of growth retardation. Indeed, this difference disappeared over 12 weeks of the standard diet or HFD (Fig. 2*C* and *D*), resulting in a comparable weight gain (Fig. 2*B* and Supplementary Fig. 1*A*) because the increase in lean mass (Fig. 2*C*) was counterbalanced by less increase in whole-body fat mass (Fig. 2*D*). HFD induced a mild fasting hyperglycemia in both Wt and $Osm^{-/-}$ mice (Fig. 2*E*), but $Osm^{-/-}$ mice showed a more severe glucose intolerance (Fig. 2*F–H*). Glucose tolerance was worsened by *Osm*

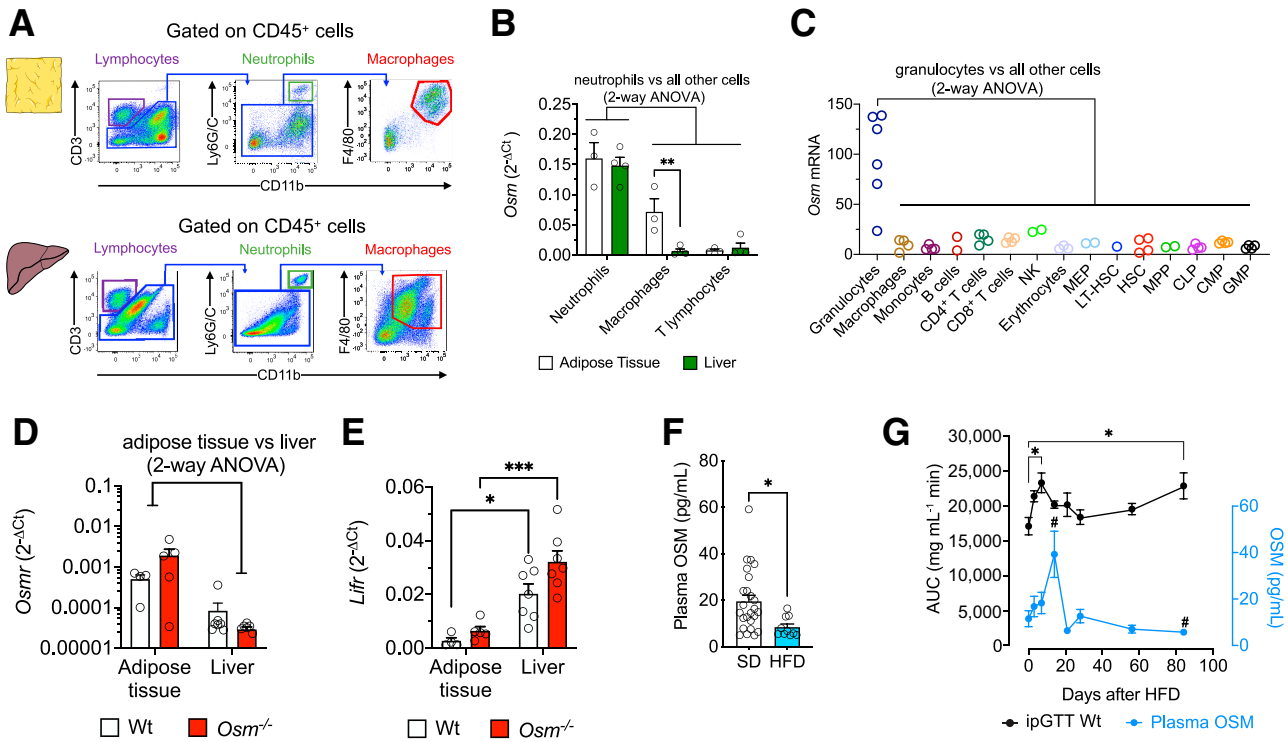

Figure 1—Sources of OSM and its modulation during obesity. (*A*) Gating strategy for FACS analysis on single-cells suspension of AT and liver. (*B*) *Osm* gene expression of sorted populations from Wt mice ($n \geq 3$/group). (*C*) *Osm* gene expression in mature leukocytes and hematopoietic progenitors as defined from single-cell RNA sequencing from the Bloodspot database. (*D* and *E*) *Osmr* and *Lifr* gene expression in the liver and in the AT ($n \geq 4$/group). (*F*) Concentration of OSM in the plasma of Wt mice after the standard diet (SD) or HFD. (*G*) Wt mice ($n = 4$) were fed the HFD and. at specific time points. ipGTT was performed and blood samples collected. The chart reports the area under the curve (AUC) of the ipGTT and the quantification of plasma OSM. #$P < 0.05$ for plasma OSM versus baseline. *$P < 0.05$, ** $P < 0.01$, *** $P < 0.001$, unless otherwise indicated. $2^{-\Delta Ct}$, comparative cycle threshold; CLP, common lymphoid progenitor; CMP, common myeloid progenitors; GMP, granulocyte-monocyte progenitor; LT-HSC, long-term hematopoietic stem cell; MEP, megakaryocyte-erythrocyte progenitors; NK, natural killer (cells).

deletion already after 1 week of an HFD, supporting an early role for OSM in modulating the metabolic response to the HFD (Supplementary Fig. 1*B*).

There was no difference in insulin sensitivity, as assessed by the ipITT (Fig. 2*I*–*K*) and confirmed by insulin concentrations and HOMA-IR values (Fig. 2*L* and *M*). Glucagon and the insulin to glucagon ratio showed similar changes in *Osm*$^{-/-}$ and Wt mice after they were fed the HFD (Supplementary Fig. 1*C* and *D*). Concentrations of glucagon-like peptide-1 (GLP-1) were strikingly lower in *Osm*$^{-/-}$ than in Wt mice fed the standard diet, suggesting impaired function of intestinal L cells (Fig. 2*N*). As a result, the expected decline in GLP-1 levels after the HFD was observed only in Wt mice (28). Levels of glucose-dependent insulinotropic peptide showed no change due to diet or genotype (Supplementary Fig. 1*E*). The HFD increased leptin, resistin, and PAI-1, and reduced ghrelin in a similar fashion in Wt and *Osm*$^{-/-}$ mice (Supplementary Fig. 1*F*–*I*). The RER showed a similar circadian variation in Wt and *Osm*$^{-/-}$ mice (Supplementary Fig. 1*J* and *K*). As early as 4 weeks after initiation of the HFD, both Wt and *Osm*$^{-/-}$ mice lost the circadian profile with the expected RER reduction (Supplementary Fig. 1*L* and *M*), indicating a shift of substrate utilization from carbohydrates to fatty acids (29). Superimposable results were obtained then the HFD was stopped (Supplementary Fig. 1*N* and *O*). Wt and *Osm*$^{-/-}$ mice had a similar energy expenditure profile, showing the expected increase at night (zeitgeber time 12–24) (Supplementary Fig. 1*P*–*T*), and during the day after eating the HFD, due to an increase in VO_2 caused by differences in substrate utilization (30).

We also measured glucose uptake in vivo. *Osm*$^{-/-}$ mice fed the standard diet had lower 2DG uptake in the liver, in AT, and in fast-twitch tibilias anterior muscle. Such differences persisted with the HFD, particularly for the tibialis anterior muscle, which showed a marked reduction of 2DG uptake in *Osm*$^{-/-}$ mice (Fig. 2*O*).

AT Tissue and Liver Remodeling

The HFD resulted in increased median cross-sectional area (CSA) of adipocytes and skewed their distribution in a similar fashion in *Osm*$^{-/-}$ and Wt mice (Fig. 3*A*–*C*). Crown-like structures (CLSs), which represent infiltrating macrophages around dying adipocytes (31), were increased in both *Osm*$^{-/-}$ and Wt mice as a result of the HFD, without significant differences between the two groups (Fig. 3*D*). The HFD resulted in increased abundance of macrophages and neutrophils (Fig. 3*E* and *F*) in Wt and

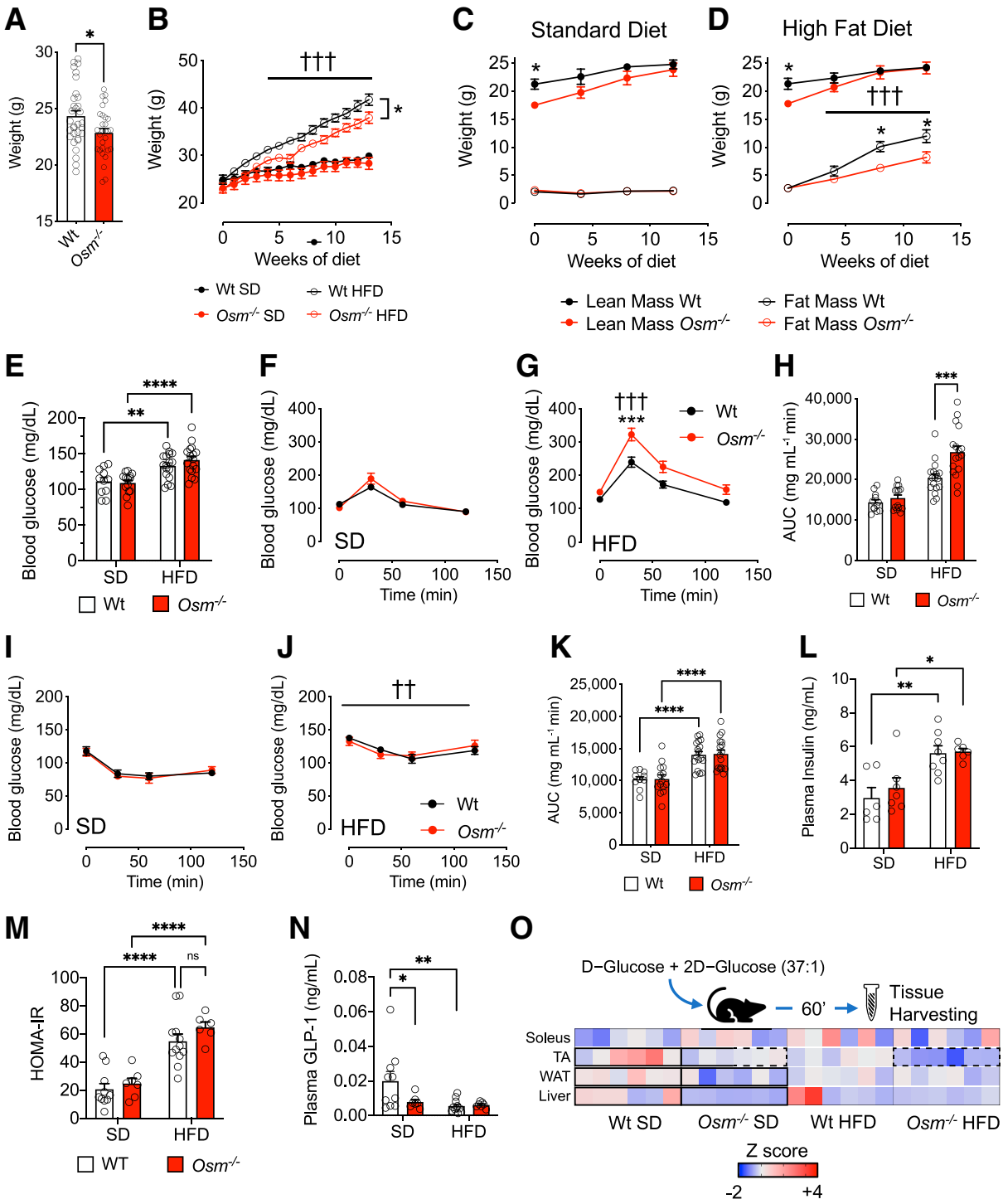

Figure 2—Body weight and metabolic characterization of *Osm* $^{-/-}$ mice after the HFD. (*A*) Baseline body weight of 8-week-old Wt and *Osm* $^{-/-}$ mice. (*B*) Body weight of Wt and *Osm* $^{-/-}$ mice fed the standard diet (SD) and the HFD ($n \geq 10$/group). †††$P < 0.001$ for standard diet versus HFD. (*C* and *D*) Body composition of Wt and *Osm* $^{-/-}$ mice fed the standard diet and the HFD ($n \geq 8$/group). †††$P < 0.001$ for the SD versus the HFD. *$P < 0.05$ for Wt versus *Osm* $^{-/-}$. (*E*) Baseline blood glucose levels of Wt and *Osm* $^{-/-}$ mice after 12 weeks of the SD or the HFD ($n \geq 10$). (*F–H*) Results of ipGTT for Wt and *Osm* $^{-/-}$ mice fed the standard diet (*F*) or HFD (*G*) with respective AUCs (*H*). ***$P < 0.001$ for Wt versus *Osm* $^{-/-}$; †††$P < 0.001$ for SD versus HFD. (*I–K*) Results of ipITT for Wt and *Osm* $^{-/-}$ mice under fed the standard diet (*I*) or HFD (*J*), with respective AUCs (*K*). ††$P < 0.01$ for standard diet versus HFD. (*L*) Plasma insulin concentration ($n \geq 6$). (*M*) HOMA-IR ($n \geq 7$). (*N*) Plasma GLP-1 concentration ($n \geq 6$). (*O*) Experimental layout and heat map of 2-DG uptake ratio of individual standard diet versus HFD Wt and *Osm* $^{-/-}$ mice. For each tissue, statistical significance is highlighted with continuous rectangles ($P < 0.05$ Wt versus *Osm* $^{-/-}$) or dashed rectangles ($P < 0.05$ standard diet versus HFD). *$P < 0.05$, **$P < 0.01$, ***$P < 0.001$, ****$P < 0.0001$. TA, tibilias anterios muscle; WAT, white adipose tissue.

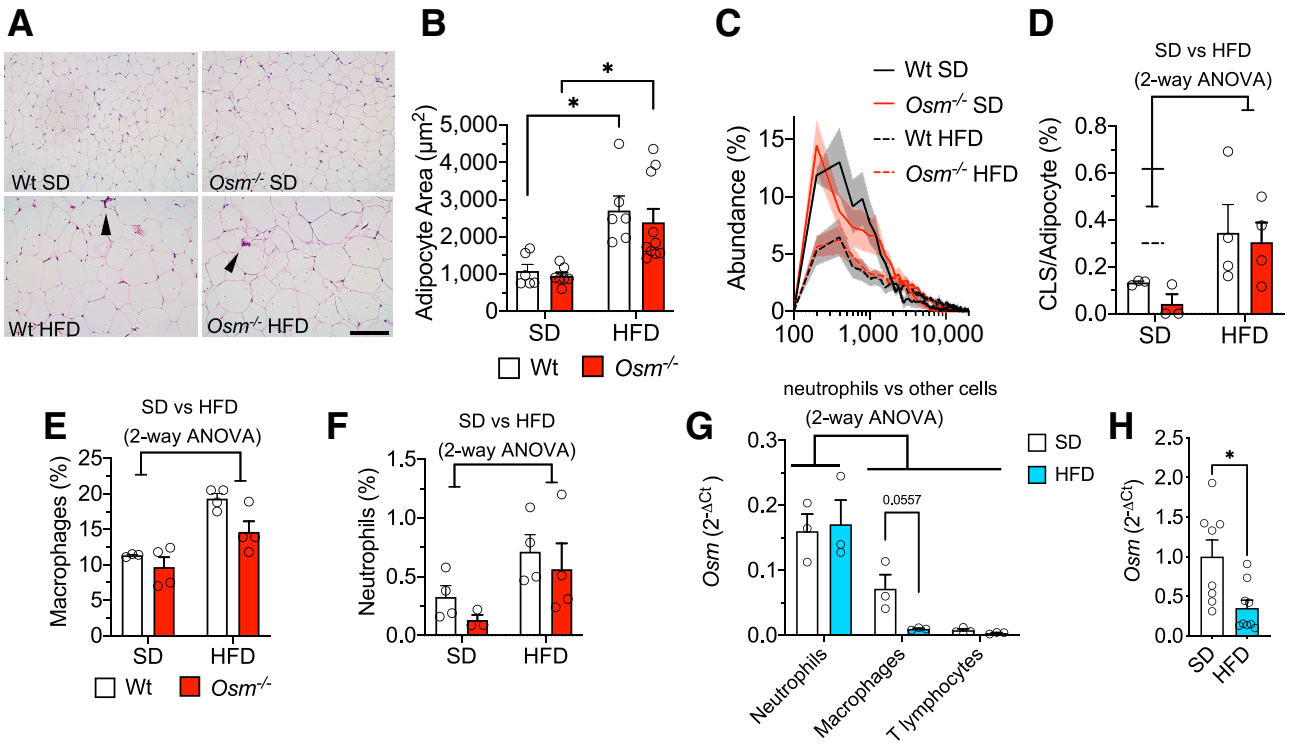

Figure 3—Visceral AT remodeling after the HFD regimen. (*A*) Hematoxylin and eosin staining of visceral AT from Wt and *Osm* $^{-/-}$ mice on fed the standard diet (SD) or HFD. The arrows indicate CLSs (scale bar: 120 µm). (*B*) Adipocyte CSA quantifications ($n \geq 6$/group). (*C*) Distribution of adipocyte area (on a log scale) from Wt and *Osm* $^{-/-}$ mice fed the standard diet or HFD. (*D*) Ratio of CLSs to adipocytes in the four groups ($n \geq 4$/group). (*E* and *F*) Quantification of macrophages and neutrophils with flow cytometry ($n \geq 3$/group). (*G*) *Osm* gene expression of sorted populations after the HFD ($n = 3$/group). (*H*) *Osm* gene expression of unfractionated visceral AT ($n > 7$ group). *$P < 0.05$. $2^{-\Delta Ct}$, comparative cycle threshold.

Osm $^{-/-}$ mice to a similar extent, but *Osm* $^{-/-}$ mice had less accumulation of T lymphocytes than the Wt mice (Supplementary Fig. 2*A*).

Macrophages were the most abundant inflammatory cells in AT and they likely contributed to the majority of OSM gene expression of AT. Consistently, the HFD resulted in reduced *Osm* expression in macrophages (Fig. 3*G*), matching reduced *Osm* expression in AT (Fig. 3*H*). Deletion of *Osm* did not impinge upon macrophage phenotype, as assessed by in vitro polarization of BM-derived macrophages (Supplementary Fig. 2*B*–*D*). *Osmr* and *Lifr* mRNA levels in AT were significantly higher in standard diet *Osm* $^{-/-}$ mice compared with Wt mice, whereas the HFD abolished these differences (Supplementary Fig. 2*E* and *F*).

In the liver, ORO staining showed expected lipid accumulation induced by the HFD (Fig. 4*A*) without evidence of fibrosis (Supplementary Fig. 3*A*). Liver triglyceride content was lower in *Osm* $^{-/-}$ mice than in Wt mice under the HFD regimen (Fig. 4*B*), with no difference in cholesterol content (Supplementary Fig. 3*B*). The core enrichment of several genes involved in lipid homeostasis was deregulated in HFD *Osm* $^{-/-}$ mice compared with Wt mice (Fig. 4*C*).

Il6 mRNA concentration was higher in *Osm* $^{-/-}$ than in Wt mice under both the standard diet and HFD regimens, and *Il1b* mRNA concentration was increased by HFD in *Osm* $^{-/-}$ mice compared with Wt mice (Fig. 4*D* and *E*). The HFD resulted in increased abundance of liver macrophages, but not of T lymphocytes, similarly in the two groups (Fig. 4*F*, and Supplementary Fig. 3*C*), and neutrophils were increased as a result of the HFD only in Wt mice, not in *Osm* $^{-/-}$ (Fig. 4*G*). *Osm* expression was not modified by the HFD in inflammatory cells and at tissue level (Supplementary Fig. 3*D* and *E*). *Osmr* was increased as a result of the HFD only in *Osm* $^{-/-}$ mice (Supplementary Fig. 3*F*), whereas *Lifr* expression was similar among experimental groups (Supplementary Fig. 3*G*). Serum levels of AST were increased in *Osm* $^{-/-}$ mice fed the HFD (Fig. 4*H*), as a sign of hepatic inflammation and metabolic impairment (32). Furthermore, OSM deletion induced a small increase in serum triglyceride levels independently of the diet, with no difference in the increase of serum cholesterol between Wt and *Osm* $^{-/-}$ mice (Supplementary Fig. 3*H* and *I*). Plasma free fatty acids showed no difference (Supplementary Fig. 3*J*).

In summary, deletion of *Osm* induced no overt change in adiposity due to the HFD, but it worsened liver inflammation and damage. Analysis of single-cell sequencing of the data set (33) showed that *Osmr* in the liver and AT was expressed almost exclusively by stromal and endothelial cells (Supplementary Fig. 4) suggesting that metabolic

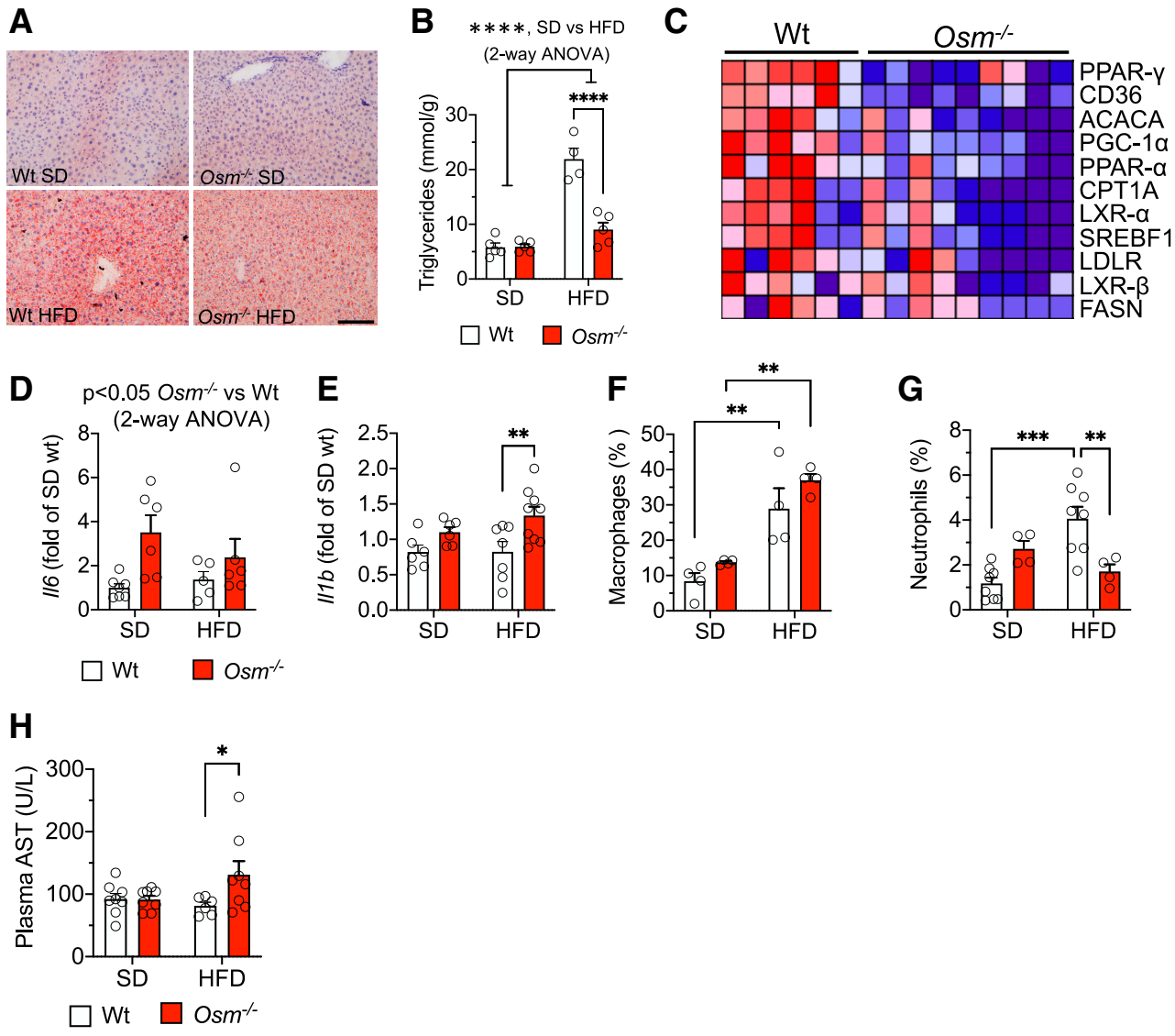

Figure 4—Liver remodeling after the HFD regimen. ORO staining of liver cryosections (scale bar: 120 μm) (*A*) and triglyceride quantification (*B*); $n \geq 4$/group. (*C*) GSEA heat map of differentially expressed genes in HFD livers. (*D* and *E*) Gene expression of *Il6* and *Il1b*. (*F* and *G*) Quantification of macrophages and neutrophils with flow cytometry ($n \geq 3$/group). (*H*) Blood chemistry of the four experimental groups measuring AST. $^{**}P < 0.01$, $^{***}P < 0.001$, $^{****}P < 0.0001$. SD, standard diet.

effects of OSM might be due to a cross talk between immune cells and the stroma of such organs.

Effects of Hematopoietic *Osm* Deletion on Responses to HFD

We performed BM transplantation (BMT) experiments to assess whether postnatal deletion of *Osm* in hematopoietic cells recapitulated the metabolic phenotype of constitutive whole-body *Osm*$^{-/-}$ mice (Fig. 5*A*). After myeloablation, 3-month-old Wt male mice were transplanted with either Wt (BMT^{Wt}) or *Osm*$^{-/-}$ (BMT^{OsmKO}) BM cells, which yielded a similar degree of reconstitution (Supplementary Fig. 5*A* and *B*), as we have previously shown (34). Accordingly, in BMT^{OsmKO} mice, plasma OSM was reduced to ~20% the level seen in BMT^{Wt} mice (3.9 ± 0.4 pg/mL vs. 18.5 ± 4.1 pg/mL; $P < 0.05$). As reported for Wt mice, plasma OSM declined after HFD in BMT^{Wt} mice (Fig. 5*B*), suggesting that blood cells are major contributors to systemic OSM levels. Residual detection of OSM in BMT^{OsmKO} mice might be due to long-lived tissue-resident cells of monocyte/macrophage lineage that persist after radiative myeloablation (35–37). The HFD had a similar impact on body weight and whole-body composition in BMT^{Wt} and BMT^{OsmKO} mice (Fig. 5*C* and Supplementary Fig. 5*C* and *D*). According to these data, we ruled out that hematopoietic-derived OSM is a major regulator of fat accumulation and weight gain induced by the HFD.

Blood glucose levels were slightly higher in BMT^{OsmKO} mice fed the standard diet, though the difference did not reach statistical significance despite adequate sample size

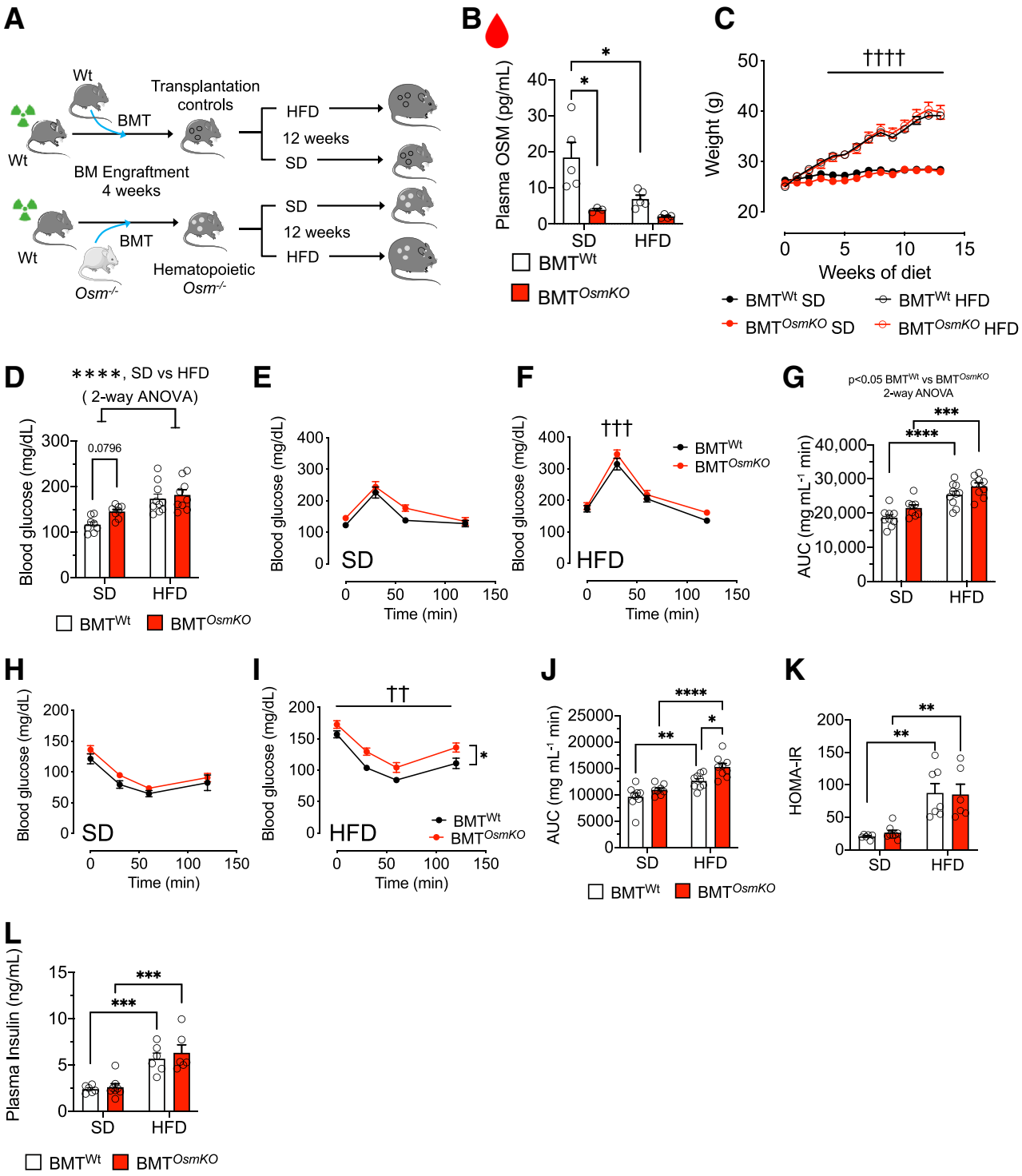

Figure 5—Generation of hematopoietic-restricted *Osm* $^{-/-}$ mice and metabolic characterization after HFD. (*A*) Experimental overview of BMT: Wt mice were transplanted with *Osm* $^{-/-}$ and Wt BM (BMT^{Wt} and BMT^{OsmKO}, respectively) and subsequently underwent HFD feeding. (*B*) Concentration of OSM in the plasma ($n \geq 5$/group). (*C*) Body weight of BMT^{Wt} and BMT^{OsmKO} mice fed the standard diet (SD) and HFD ($n \geq 8$/group). ††††$P < 0.001$ for SD versus HFD. (*D*) Baseline blood glucose levels of BMT^{Wt} and BMT^{OsmKO} mice after 12 weeks of SD or HFD ($n \geq 8$). (*E–G*) Results of ipGTT for BMT^{Wt} and BMT^{OsmKO} mice fed the SD (*E*) and HFD (*F*), with respective AUCs (*G*). †††$P < 0.001$ for SD versus HFD. (*H–J*) Results of ipITT of BMT^{Wt} and BMT^{OsmKO} mice fed the SD (*H*) and HFD (*I*), with respective AUCs (*J*). ††$P < 0.01$ for SD versus HFD. (*K*) HOMA-IR ($n \geq 5$). (*L*). Plasma insulin concentration ($n \geq 5$). *$P < 0.05$, **$P < 0.01$, ***$P < 0.001$, ****$P < 0.0001$.

(Fig. 5*D*) (145.2 ± 4.99 mg/dL vs. 116.6 ± 6.04 mg/dL; $n = 8$; $P = 0.08$). Glucose intolerance was induced by the HFD in both BMT^{OsmKO} and BMT^{Wt} mice (Fig. 5*E–G*), but the analysis of area under the curve (AUC) from ipGTTs showed a significant effect of both diet and genotype, suggesting that a worse baseline glucose intolerance of BMT^{OsmKO} mice was further exacerbated by the HFD (Fig. 5*G*). BMT^{OsmKO} mice at the end of the HFD regimen also had slightly worse insulin sensitivity than the BMT^{Wt} animals (Fig. 5*H–J*), despite similar insulin concentrations and HOMA-IR (Fig. 5*K* and *L*). Changes of RER, glucose uptake, and energy expenditure due to the HFD were similar in the two groups of BMT animals (Supplementary Fig. 6*A–K*).

AT and Liver Remodeling in BMT^{Wt} and BMT^{OsmKO} Mice

The HFD resulted in increased adipocyte median CSAs (Fig. 6*A* and *B*), right-skewed their distribution (Fig. 6*C*) and increased the number of CLSs per adipocyte similarly in BMT^{Wt} and BMT^{OsmKO} mice (Fig. 6*D*). *Osm* expression in

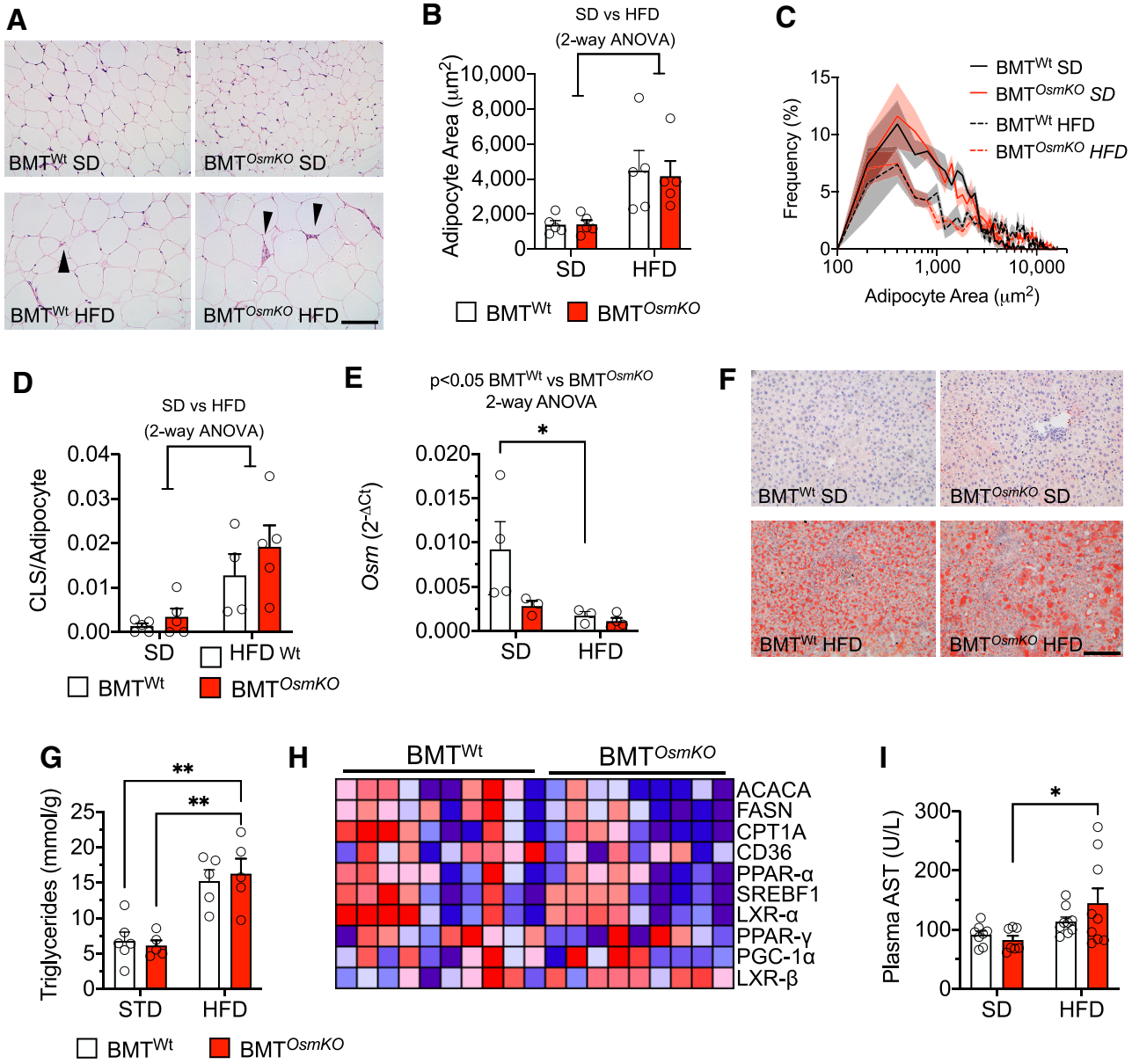

Figure 6—Visceral AT and liver remodeling after the HFD regimen in BMT^{Wt} and BMT^{OsmKO} mice. (*A*) Hematoxylin and eosin staining of visceral AT from BMT^{Wt} and BMT^{OsmKO} mice fed the standard diet (SD) or HFD. The arrows indicate CLSs (scale bar: 120 μm). (*B*) Adipocyte CSA quantifications ($n \geq 5$/group). (*C*) Distribution of adipocyte area (on a log scale) from BMT^{Wt} and BMT^{OsmKO} mice fed the SD or HFD. (*D*) Ratio of CLSs to adipocytes in the four groups ($n \geq 4$/group). (*E*) *Osm* gene expression of unfractionated visceral AT ($n \geq 5$ group). (*F* and *G*) ORO staining of liver cryosections (scale bar: 120 μm) (*F*) and triglyceride quantification (*G*); $n \geq 4$/group. (*H*) GSEA heat map of differentially expressed genes in HFD livers. (*I*) AST measurements of the four experimental groups. *$P < 0.05$, **$P < 0.01$. $2^{-\Delta Ct}$, comparative cycle threshold.

AT was reduced by the HFD in BMT^{Wt} mice, with a small residual expression in BMT^{OsmKO} mice (Fig. 6*E*), matching plasma OSM concentration (Fig. 5*B*). Leptin, resistin, and PAI-1 levels were increased as a result of the HFD, ghrelin showed no variations, GLP-1 concentrations were low in all groups, and glucose-dependent insulinotropic peptide levels were slightly increased in BMT^{OsmKO} (Supplementary Fig. 7*A–F*). ORO staining and triglyceride quantification in the liver showed similar effects of the HFD in both BMT^{Wt} and BMT^{OsmKO} mice (Fig. 6*F* and *G*), without signs of fibrosis or changes in total cholesterol level (Supplementary Fig. 7*G* and *H*). The core enrichment for genes involved in lipid homeostasis displayed no striking differences between BMT^{Wt} and BMT^{OsmKO} mice (Fig. 6*H*). Of note, hematopoietic-restricted OSM deletion recapitulated the increase in AST observed in whole-body *Osm*$^{-/-}$ mice after the HFD regimen (Fig. 6*I*). Elevations in plasma cholesterol and triglyceride levels were equally observed in BMT^{Wt} and BMT^{OsmKO} mice fed the HFD (Supplementary Fig. 7*I* and *J*) without changes in FFAs (Supplementary Fig. 7*K*). Expression of *Osm*, *Osmr*, and *Lifr* showed no difference due to either diet or the BMT in the AT or the liver (Supplementary Fig. 7*L–P*).

Altogether, these data show that hematopoietic cells were major contributors to *Osm* expression and OSM concentrations in plasma, liver, and AT. Moreover, postnatal, hematopoietic-restricted *Osm* deletion recapitulated glucose intolerance and liver damage due to whole-body *Osm* deletion.

Attempt to Rescue Hematopoietic *Osm* Phenotype

We finally transplanted Wt and *Osm*$^{-/-}$ BM cells into lethally irradiated *Osm*$^{-/-}$ recipients (KO^{BMTWt} and KO^{BMTKO}, respectively) (Fig. 7*A*). Successful engraftment was confirmed by peripheral blood cell count and flow cytometry analysis of the BM (Supplementary Fig. 8*A–E*). The HFD induced a modest weight gain in both KO^{BMTWt} and KO^{BMTKO} mice (Fig. 7*B*) and a significant increase in whole-body fat mass

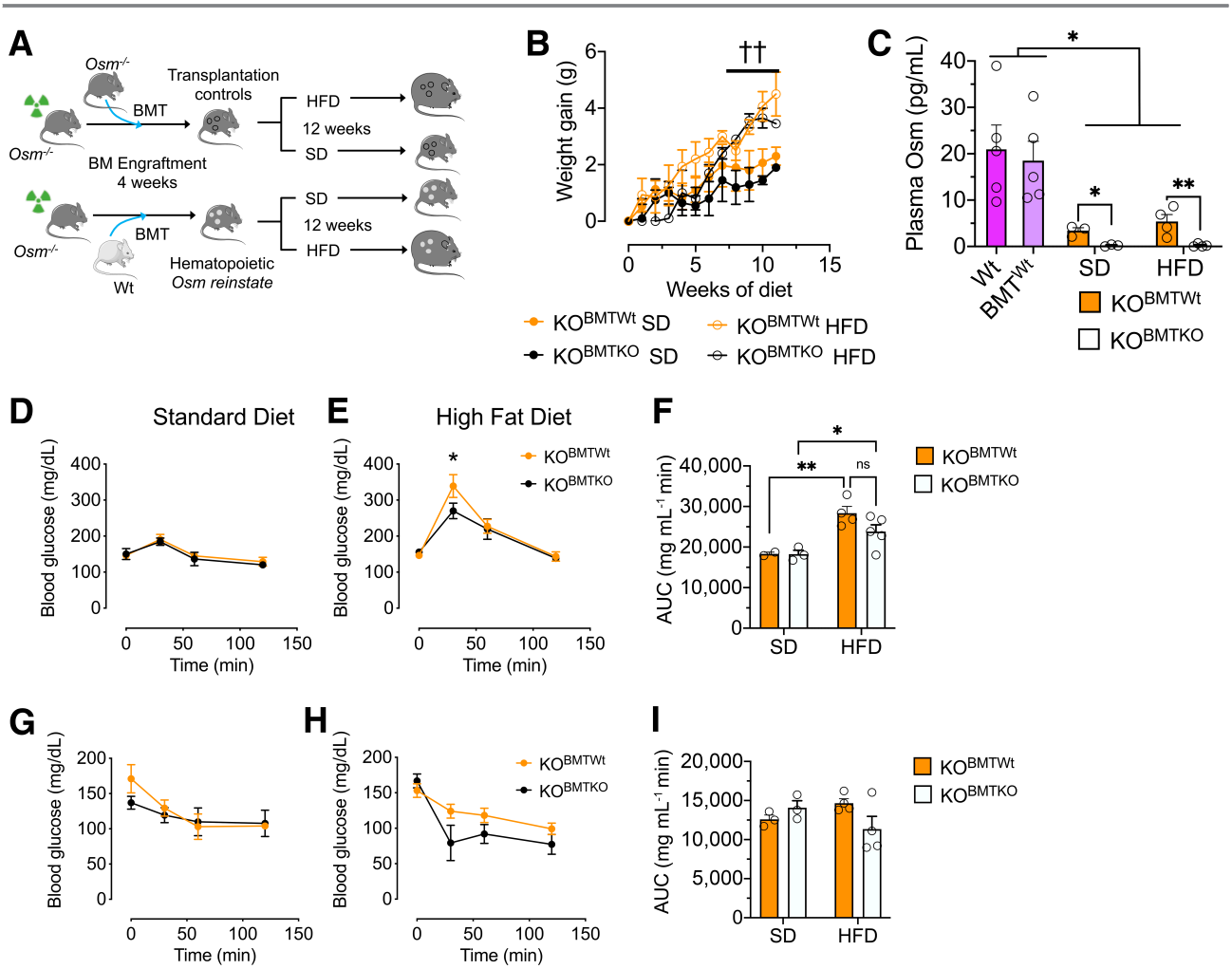

Figure 7—Hematopoietic OSM reconstitution and metabolic characterization after the HFD regimen. (*A*) Experimental overview of BMT: *Osm*$^{-/-}$ mice were transplanted with Wt BM (KO^{BMTWt}) and *Osm*$^{-/-}$ BM (KO^{BMTKO}), followed by HFD feeding. (*B*) Weight gain of mice fed the standard diet (SD) and HFD ($n \geq 3$/group). ††$P < 0.01$ for SD versus HFD. (*C*) Concentration of OSM in the plasma. (*D–F*) ipGTT of transplanted mice fed the SD (*D*) or HFD (*E*) with respective areas under the curve (AUCs) *F*. (*G–I*) Results of ipITT of transplanted mice fed the SD (*G*) or HFD (*H*) with respective AUCs (*I*). *$P < 0.05$, **$P < 0.01$.

(Supplementary Fig. 9*A* and *B*) but no evidence of excess myelopoiesis (Supplementary Fig. 9*C* and *D*). Plasma OSM concentrations were expectedly higher in KO^{BMTWt} mice than in KO^{BMTKO} mice but remained fivefold lower than in Wt or BMT^{Wt} mice and unaffected by the HFD (Fig. 7*C*). Therefore, rescue of OSM levels was far from complete. The HFD induced glucose intolerance and insulin resistance similarly in KO^{BMTWt} and KO^{BMTKO} mice, with no difference in AUC based on donor cell type (Fig. 7*D–I*). These data indicate that, despite full hematopoietic reconstitution, transplantation of Wt cells into $Osm^{-/-}$ mice did not replenish full OSM secretion and did not rescue metabolic dysfunction of $Osm^{-/-}$ mice.

DISCUSSION

OSM has been claimed to be responsible for both proinflammatory and anti-inflammatory actions (38,39). Therefore, it is not surprising that its role in obesity and type 2 diabetes is disputed. Here, we show that OSM is mainly produced by macrophages and neutrophils in the blood and tissues and undergoes modulation during a HFD regimen, with an early surge followed by a chronic reduction. This dynamic modulation can be interpreted as an adaptive response affecting the metabolic status because whole-body *Osm* deletion worsened glucose tolerance from the first weeks of the HFD regimen. Notably, deletion of *Osm* in adult hematopoietic cells was sufficient to induce glucose intolerance, mimicking constitutive whole-body $Osm^{-/-}$ deletion. Data obtained from hematopoietic-restricted $Osm^{-/-}$ mice confirmed that blood cells are the major source of OSM in plasma, liver, and AT, suggesting these mice accurately show the net metabolic effects of inhibiting OSM postnatally.

Despite successful engraftment, the transplantation of Wt BM cells into $Osm^{-/-}$ mice (KO^{BMTWt}) yielded low plasma OSM and, consequently, failed to improve metabolic derangement induced by the HFD. Tissue-resident macrophages can persist after irradiation and BMT and are scarcely renewed by circulating cells (40). They are known to release OSM to recruit OSM-producing neutrophils in a paracrine loop needed for tissue regeneration and homeostasis (41). Therefore, we hypothesize that in KO^{BMTWt} mice, $Osm^{-/-}$ tissue-resident macrophages failed to elicit the paracrine activity required for instructing Wt cells to release OSM, thus explaining the persistently low plasma OSM concentrations. Conversely, by transplanting $Osm^{-/-}$ BM into Wt mice, even if tissue-resident Wt macrophages still produced OSM, recruited immune cells would be devoid of OSM, thus recapitulating the metabolic phenotype of $Osm^{-/-}$ mice. Recruitment of neutrophils in the liver is driven by AT macrophages (42), which also emerge as a major source of OSM that could be instrumental in establishing a meta-inflammatory cross talk between AT and the liver. Indeed, the number of neutrophils was reduced in the liver of $Osm^{-/-}$ mice after the HFD regimen, where we observed the most striking effect of *Osm* deletion.

Reduction of *Osm* expression in AT after the HFD regimen was paralleled by reduction in OSM plasma levels. This finding is consistent with AT-infiltrating hematopoietic cells being the major source of AT *Osm*. This finding apparently contrasts with prior reports showing increased OSM in AT of different models of obesity but, at the same time, favorable metabolic effects of high-dose OSM administration (12). Although this counterintuitive result may reflect a form of OSM resistance that can be overcome with high OSM doses, we have shown that treatment with OSM activates myelopoiesis (34), suggesting caution in pursuing OSM as a treatment for metabolic diseases. In humans, levels of OSM in the subcutaneous AT have been reported to correlate inversely with glucose disposal, indirectly suggesting that elevated OSM in AT promotes metabolic dysfunction (14). This association, however, does not necessarily imply that OSM impairs metabolism because it can be also explained as a compensatory response to the worsening metabolic status. Furthermore, the metabolic significance of subcutaneous AT is different from that of visceral AT (43), and additional studies in humans are warranted to dissect this point.

In type 1 diabetes, we discovered a pathway whereby hyperglycemia increased *Osm* expression that, in turn, sustained myelopoiesis and impaired HSC mobilization (34). Hence, OSM inhibition may provide short-term benefit for stem cell-mediated tissue homeostasis. In type 2 diabetes and obesity, OSM is likely subjected to different layers of regulation uncoupled from hyperglycemia, including microbial triggers (44). Our new data in HFD mice suggest that OSM inhibition may have detrimental metabolic effects that can persist long term.

A role for OSM in hepatic lipid metabolism has been proposed, but the net effect is difficult to predict because OSM downregulates both CPT-1a and FAS, thus modulating both fatty acid oxidation and synthesis (45). Possibly due to their lesser fat mass, $Osm^{-/-}$ mice fed the HFD had reduced steatosis (12,13,19,20), while showing increased inflammatory gene expression and signs of liver damage. These mixed results might derive from a multiplicity of pathways activated by OSM, as well as from long-term adaptations to constitutive whole-body *Osm* deletion. In fact, hepatic lipid accumulation induced by the HFD was not modified in BMT^{OsmKO} mice. OSM is required for development of the fetal liver, which is also the major site of antenatal hematopoiesis (46). Reduced steatosis in $Osm^{-/-}$ liver might also result from altered intestinal lipid absorption, given the role of OSM in modulating the gut barrier function (39).

The literature is inconsistent on the effects of the HFD on OSMRβ, which we found was expressed at low levels in AT and liver. Data from $Osmr\beta^{-/-}$ mice support our findings (12), but the metabolic effects of OSM in vivo may be indirect, because OSMRβ in the liver and in AT is expressed mainly by endothelial and stromal cells (16). Indeed, the metabolic phenotype of $OSMR^{FKO}$ mice is rather mild (16,17). It is also possible that adipocyte OSMRβ acts as a decoy receptor to buffer OSM concentration at the tissue level (47).

As a limitation, we acknowledge we are still missing the exact mechanism whereby OSM regulates the metabolic response to the HFD. Although insulin sensitivity was unaffected, glucose tolerance was consistently worsened by constitutive whole-body and adult, hematopoietic-restricted *Osm* deletion. Along with the reduction in muscle and liver glucose uptake, these data suggest that OSM may promote glucose disposal. OSM stimulates GLP-1 expression by ileal L cells, an effect supposed to potentiate insulin secretion (15). In agreement with this, $Osm^{-/-}$ mice had remarkably lower levels of GLP-1, which could contribute to glucose intolerance after the HFD. Indeed, although mice lacking *Glp1r* have normal oral glucose tolerance, mice with selective deletion of β-cell *Glp1r* have impaired intraperitoneal glucose tolerance (48). Therefore, the interplay between OSM and the incretin effect is worth exploring in future studies.

The plethora of pathways influenced by OSM, its dynamic regulation over time, and the tissue specificity of OSM's effects are evident from our results. Dissecting these pathways will require targeted and conditional knock-out models to ablate OSM or its receptors from several relevant cell populations, including intestinal cells and β-cells.

In conclusion, we found that OSM undergoes a dynamic regulation during development of obesity-associated metabolic dysfunction, and we propose that the coordinated release of OSM by blood cells is part of a physiological response to an HFD, contributing to metabolic homeostasis.

Acknowledgments. The authors thank Kenneth A. Dyar (Institute for Diabetes and Cancer, Helmholtz Diabetes Center, Helmholtz Zentrum Munich) for copyediting and proofreading the manuscript.

Funding. This study was supported by a grant from GlaxoSmithKline, a grant from the University of Padova to M.A. (Finanziato dall'Unione Europea – NextGenerationEU, STARS@UNIPD MalTraDiates), and grants to G.P.F. (PNRR M4C2-Investimento 1.4-CN00000041 Finanziato dall'Unione Europea – NextGenerationEU; PRIN 2017-93XZ5A [Metabolic therapy of immuno-inflammation]).

Duality of Interest. M.A., S.C., and G.P.F. are the inventors of a patent (EP3197480), held by the University of Padova, on the use of pharmacologic OSM inhibition to allow stem cell mobilization. No other potential conflicts of interest relevant to this article were reported.

The external sponsor had no role in the study design, conduction, data analysis, interpretation, and decision to publish.

Author Contributions. M.A. designed and performed experiments, researched and analyzed data, provided funding and wrote the manuscript. S.C., A.R., L.M., F.I.A., C.B., and G.Z. designed and performed experiments, researched and analyzed data, and revised the manuscript. A.R. designed experiments, contributed to discussion, and revised the manuscript. G.P.F. researched and analyzed data, provided supervision and funding, and wrote the manuscript. M.A. and G.P.F. are the guarantors of this work and, as such, had full access to all the data in the study and take responsibility for the integrity of the data and the accuracy of the data analysis.

Prior Presentation. Part of this work was presented at the 58th Annual Meeting of the European Association for the Study of Diabetes, Stockholm, Sweden, 19–23 September 2022.

References

1. Chatterjee S, Khunti K, Davies MJ. Type 2 diabetes. Lancet 2017;389:2239–2251
2. Sun K, Kusminski CM, Scherer PE. Adipose tissue remodeling and obesity. J Clin Invest 2011;121:2094–2101
3. Hotamisligil GS, Shargill NS, Spiegelman BM. Adipose expression of tumor necrosis factor-alpha: direct role in obesity-linked insulin resistance. Science 1993;259:87–91
4. Gregor MF, Hotamisligil GS. Inflammatory mechanisms in obesity. Annu Rev Immunol 2011;29:415–445
5. Hermanns HM. Oncostatin M and interleukin-31: cytokines, receptors, signal transduction and physiology. Cytokine Growth Factor Rev 2015;26:545–558
6. Sims NA. Cell-specific paracrine actions of IL-6 family cytokines from bone, marrow and muscle that control bone formation and resorption. Int J Biochem Cell Biol 2016;79:14–23
7. Minehata K, Takeuchi M, Hirabayashi Y, et al. Oncostatin M maintains the hematopoietic microenvironment and retains hematopoietic progenitors in the bone marrow. Int J Hematol 2006;84:319–327
8. Sato F, Miyaoka Y, Miyajima A, Tanaka M. Oncostatin M maintains the hematopoietic microenvironment in the bone marrow by modulating adipogenesis and osteogenesis. PLoS One 2014;9:e116209
9. Albiero M, Poncina N, Ciciliot S, et al. Bone marrow macrophages contribute to diabetic stem cell mobilopathy by producing oncostatin M. Diabetes 2015;64:2957–2968
10. Tedesco S, Ciciliot S, Menegazzo L, et al. Pharmacologic PPAR-γ activation reprograms bone marrow macrophages and partially rescues HSPC mobilization in human and murine diabetes. Diabetes 2020;69:1562–1572
11. Miyaoka Y, Tanaka M, Naiki T, Miyajima A. Oncostatin M inhibits adipogenesis through the RAS/ERK and STAT5 signaling pathways. J Biol Chem 2006;281:37913–37920
12. Komori T, Tanaka M, Senba E, Miyajima A, Morikawa Y. Deficiency of oncostatin M receptor β (OSMRβ) exacerbates high-fat diet-induced obesity and related metabolic disorders in mice. J Biol Chem 2014;289:13821–13837
13. Komori T, Tanaka M, Senba E, Miyajima A, Morikawa Y. Lack of oncostatin M receptor β leads to adipose tissue inflammation and insulin resistance by switching macrophage phenotype. J Biol Chem 2013;288:21861–21875
14. Sanchez-Infantes D, White UA, Elks CM, et al. Oncostatin M is produced in adipose tissue and is regulated in conditions of obesity and type 2 diabetes. J Clin Endocrinol Metab 2014;99:E217–E225
15. Komori T, Tanaka M, Furuta H, Akamizu T, Miyajima A, Morikawa Y. Oncostatin M is a potential agent for the treatment of obesity and related metabolic disorders: a study in mice. Diabetologia 2015;58:1868–1876
16. Elks CM, Zhao P, Grant RW, et al. Loss of oncostatin M signaling in adipocytes induces insulin resistance and adipose tissue inflammation in vivo. J Biol Chem 2016;291:17066–17076
17. Stephens JM, Bailey JL, Hang H, et al. Adipose tissue dysfunction occurs independently of obesity in adipocyte-specific oncostatin receptor knockout mice. Obesity (Silver Spring) 2018;26:1439–1447
18. Piquer-Garcia I, Campderros L, Taxerås SD, et al. A role for oncostatin M in the impairment of glucose homeostasis in obesity. J Clin Endocrinol Metab 2020;105:e337–e348
19. Henkel J, Gärtner D, Dorn C, et al. Oncostatin M produced in Kupffer cells in response to PGE2: possible contributor to hepatic insulin resistance and steatosis. Lab Invest 2011;91:1107–1117
20. Luo P, Wang PX, Li ZZ, et al. Hepatic oncostatin M receptor β regulates obesity-induced steatosis and insulin resistance. Am J Pathol 2016;186:1278–1292
21. Ichihara M, Hara T, Kim H, Murate T, Miyajima A. Oncostatin M and leukemia inhibitory factor do not use the same functional receptor in mice. Blood 1997;90:165–173
22. Walker EC, McGregor NE, Poulton IJ, et al. Oncostatin M promotes bone formation independently of resorption when signaling through leukemia inhibitory factor receptor in mice. J Clin Invest 2010;120:582–592

23. Cipriani C, Colangelo L, Santori R, et al. The interplay between bone and glucose metabolism. Front Endocrinol (Lausanne) 2020;11:122
24. Ciciliot S, Albiero M, Menegazzo L, et al. p66Shc Deletion or deficiency protects from obesity but not metabolic dysfunction in mice and humans. Diabetologia 2015;58:2352–2360
25. Weir JB. New methods for calculating metabolic rate with special reference to protein metabolism. J Physiol 1949;109:1–9
26. Liu Z, Gu Y, Shin A, Zhang S, Ginhoux F. Analysis of myeloid cells in mouse tissues with flow cytometry. STAR Protoc 2020;1:100029
27. Bagger FO, Kinalis S, Rapin N. BloodSpot: a database of healthy and malignant haematopoiesis updated with purified and single cell mRNA sequencing profiles. Nucleic Acids Res 2019;47(D1):D881–D885
28. Richards P, Pais R, Habib AM, et al. High fat diet impairs the function of glucagon-like peptide-1 producing L-cells. Peptides 2016;77:21–27
29. Tschöp MH, Speakman JR, Arch JR, et al. A guide to analysis of mouse energy metabolism. Nat Methods 2011;9:57–63
30. Nelson DW, Gao Y, Spencer NM, Banh T, Yen CL. Deficiency of MGAT2 increases energy expenditure without high-fat feeding and protects genetically obese mice from excessive weight gain. J Lipid Res 2011;52: 1723–1732
31. Crewe C, An YA, Scherer PE. The ominous triad of adipose tissue dysfunction: inflammation, fibrosis, and impaired angiogenesis. J Clin Invest 2017;127:74–82
32. Kang HS, Liao G, DeGraff LM, et al. CD44 plays a critical role in regulating diet-induced adipose inflammation, hepatic steatosis, and insulin resistance. PLoS One 2013;8:e58417
33. The Tabula Muris Consortium, Overall Coordination, Logistical Coordination, et al. Single-cell transcriptomics of 20 mouse organs creates a Tabula Muris. Nature 2018;562:367–372
34. Albiero M, Ciciliot S, Tedesco S, et al. Diabetes-associated myelopoiesis drives stem cell mobilopathy through an OSM-p66Shc signaling pathway. Diabetes 2019;68:1303–1314
35. Nishiyama K, Nakashima H, Ikarashi M, et al. Mouse CD11b+Kupffer cells recruited from bone marrow accelerate liver regeneration after partial hepatectomy. PLoS One 2015;10:e0136774
36. Soysa R, Lampert S, Yuen S, et al. Fetal origin confers radioresistance on liver macrophages via $p21^{cip1/WAF1}$. J Hepatol 2019;71:553–562
37. Heylmann D, Ponath V, Kindler T, Kaina B. Comparison of DNA repair and radiosensitivity of different blood cell populations. Sci Rep 2021;11:2478
38. Wahl AF, Wallace PM. Oncostatin M in the anti-inflammatory response. Ann Rheum Dis 2001;60(Suppl. 3):iii75–iii80
39. West NR, Hegazy AN, Owens BMJ, et al.; Oxford IBD Cohort Investigators. Oncostatin M drives intestinal inflammation and predicts response to tumor necrosis factor-neutralizing therapy in patients with inflammatory bowel disease. Nat Med 2017;23:579–589
40. Hashimoto D, Chow A, Noizat C, et al. Tissue-resident macrophages self-maintain locally throughout adult life with minimal contribution from circulating monocytes. Immunity 2013;38:792–804
41. Lörchner H, Pöling J, Gajawada P, et al. Myocardial healing requires Reg3β-dependent accumulation of macrophages in the ischemic heart. Nat Med 2015;21:353–362
42. Bijnen M, Josefs T, Cuijpers I, et al. Adipose tissue macrophages induce hepatic neutrophil recruitment and macrophage accumulation in mice. Gut 2018;67:1317–1327
43. Schoettl T, Fischer IP, Ussar S. Heterogeneity of adipose tissue in development and metabolic function. J Exp Biol 2018;221(Suppl. 1):jeb162958
44. Headland SE, Dengler HS, Xu D, et al. Oncostatin M expression induced by bacterial triggers drives airway inflammatory and mucus secretion in severe asthma. Sci Transl Med 2022;14:eabf8188
45. Komori T, Morikawa Y. Oncostatin M in the development of metabolic syndrome and its potential as a novel therapeutic target. Anat Sci Int 2018;93: 169–176
46. Kamiya A, Kinoshita T, Ito Y, et al. Fetal liver development requires a paracrine action of oncostatin M through the gp130 signal transducer. EMBO J 1999;18:2127–2136
47. Elks CM, Stephens JM. Oncostatin M modulation of lipid storage. Biology (Basel) 2015;4:151–160
48. Smith EP, An Z, Wagner C, et al. The role of β cell glucagon-like peptide-1 signaling in glucose regulation and response to diabetes drugs. Cell Metab 2014;19:1050–1057